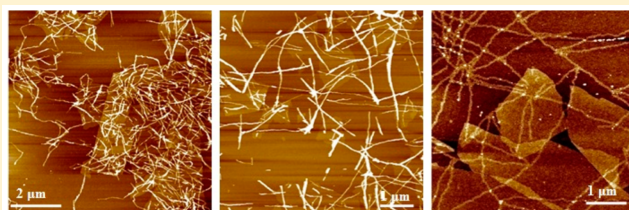


## Nanostructure-Dependent Interfacial Interactions between Poly(3-hexylthiophene) and Graphene Oxide

Sanrong Liu, Xiaojing Ma,\* Bo Wang, Xudong Shang, Wenliang Wang, and Xifei Yu\*

The Polymer Composites Engineering Laboratory, Changchun Institute of Applied Chemistry, Chinese Academy of Sciences, Changchun 130022, China

**ABSTRACT:** Poly(3-hexylthiophene) (P3HT) nanofibers with different nanostructures and intrachain order were prepared, and the interactions between different P3HT nanofibers and GO were investigated by UV-vis, Raman, and atomic force microscopy (AFM) measurements, etc. We found that at the liquid–GO interface the conjugated length of nanofibers with lower intrachain order increased since polymer chains fractions were more likely to be involved in the formation of the nanofibers. We also demonstrated that GO can be differently doped when interacting with different P3HT nanofibers, which were confirmed by Raman spectroscopy and AFM. Kelvin probe force microscopy (KPFM) was also used to monitor the surface potential (SP) change of P3HT nanofibers after they interacted with GO and further confirmed the varied interactions between different P3HT nanofibers and GO.



### INTRODUCTION

Graphene oxide (GO) are featured by  $sp^2$  conjugated domains interspersed with polar oxygenated domains and two drastically different length scales with their thinnest thickness determined to be one single atomic layers and the lateral sizes ranging from a few to hundreds of micrometers. The unique structures and excellent properties endow GO with the ability to mediate a range of energy and have charge transfer interactions with diverse molecules,<sup>1,2</sup> especially conjugated polymers.<sup>3,4</sup> Therefore, GO has stimulated a lot of interest in fabricating GO/polymer composites and exploring their application in device.<sup>5–8</sup>

Poly(3-hexylthiophene) (P3HT) has received much attention in scientific research and industrial applications due to its large overlap between the  $\pi$ -orbital delocalized over the polymer chains, the semicrystalline behavior, and ease of solution processability.<sup>9</sup> Because of the backbone rigidity and the immiscibility of the main chains and the side chains, P3HT molecules usually self-assemble into one-dimensional nanofibers or nanowhiskers from their solutions via the  $\pi-\pi$  interactions among the backbones, which allow for high hole mobilities.<sup>9–11</sup> It is widely recognized that the crystalline structure<sup>12</sup> and morphology<sup>13,14</sup> of P3HT significantly affect charge transport properties and consequently dominate the performance of devices. Recently, it is found that surface potential contrast, which is related work function of sample, depends sensitively on nanostructure morphology.<sup>14</sup> Therefore, a lot of efforts have been concentrated on controlling the crystalline structure and morphology of P3HT and trying to obtain new P3HT nanofibers with novel nanostructures or morphology.<sup>9,15–17</sup>

The work function of GO has been found to fall within the band gap of P3HT,<sup>18</sup> which suggests that GO/P3HT composites can be formed by charge transfer interactions.

Recently much attention has been paid to explore the application of the GO/P3HT composites in device due to their charge transfer interactions<sup>3,6,19</sup> and study the doping effect on either GO or P3HT by the counterpart.<sup>18,20</sup> For example, Stylianakis and co-workers synthesized a solution processable graphene by treatment of GO with phenyl isothiocyanate (PITC), and they found that when GO–PITC was used as electron acceptor material in P3HT bulk heterojunction photovoltaic devices, the power conversion efficiency can be enhanced to be 2 orders of magnitude compared with that of pristine P3HT.<sup>6</sup> Wang and co-workers reported that they prepared the GO/P3HT hybrid via  $\pi-\pi$  interactions between the GO and P3HT, which demonstrates broad-band absorption and enhanced photocatalytic properties.<sup>21</sup> Gao and co-workers found that the conductivity of P3HT film after being doped by a thin layer of GO can be as high as  $3.70 \text{ S m}^{-1}$ .<sup>20</sup> The interactions between GO and P3HT has endowed the composite with excellent properties, which either of them did not have. However, since the three-dimensional structures of GO/P3HT composites formed during the film preparation or in bulk materials are usually too complicated, the interactions between GO and P3HT are far from clear, and it is still a challenge to control the interactions. To gain a better understanding and controlling the interactions between P3HT and GO, the studies on the interfacial interactions of P3HT nanofiber with GO are needed. However, currently few studies about this have been reported. Only Liscio and co-workers used Kelvin probe force microscopy (KPFM) to probe the surface potential of P3HT and RGO at the nanometric scale and found that there are no

Received: April 18, 2015

Revised: July 2, 2015

Published: August 12, 2015

significant charge injection barriers between the graphene sheets and the P3HT due to the small work function difference between graphene and P3HT.<sup>18</sup> Moreover, it is expected that GO and P3HT can be doped by each other to different extents according to their respective compositions in the GO/P3HT hybrid complex.<sup>21</sup>

Motivated by recent studies on the effect of morphology on the electronic properties of P3HT aggregates and GO's wide application in the P3HT-based electric devices as discussed above, we presumed that different P3HT nanofibers will interact with GO differently. Herein, we prepared three kinds of P3HT ( $M_n = 34.3 \text{ kg mol}^{-1}$ , PDI = 1.24) nanofibers with different nanostructures and intrachain orders. In what follows, we will refer to the nanofibers prepared by dissolving P3HT in anisole and chloroform solvents (volume ratio = 4:1, abbreviated as A/CF) as 41nanofiber, nanofibers obtained in THF and chloroform (1:1, T/CF) mixture solvents as 11nanofiber, and nanofibers prepared in chloroform at low concentrations as monofiber. For the first time we systematically investigated the interactions between different P3HT nanofibers and GO by combined UV-vis and Raman with the atomic force microscopy (AFM) and Kelvin probe force microscopy (KPFM) measurements. We revealed that different doping extent occurred when different P3HT nanofibers interacted with GO. This method has offer an opportunity to elucidate the dependence of the interactions between the GO and conducting polymers on the different nanostructures of polymer, and the results also provide importance and valuable information on how to fabricate the devices with high performances.

## RESULTS AND DISCUSSION

Figure 1 shows the UV-vis absorption spectra of the P3HT solutions with different nanostructures. It can be seen that a

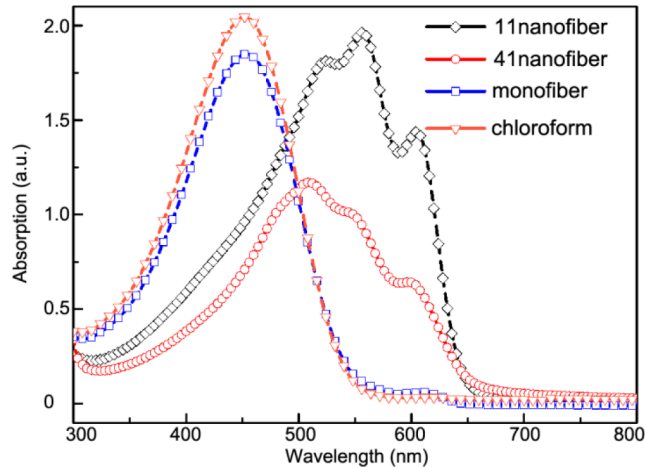


**Figure 1.** UV-vis absorption spectra of P3HT solutions with different nanostructures.

single peak at  $\lambda_{\max}$  of 454 nm appeared when P3HT was completely dissolved, whereas the absorption at 454 nm decreased accompanied by the appearance of vibronic structures at longer wavelengths (500–620 nm) when the relatively “poor” solvent was added to the “good” solvent or used to dissolve P3HT. During the fiber formation, all the solutions displayed a color change from the previous transparent yellow solution: 41nanofiber and 11nanofiber

solutions turned to be crimson, and the monofiber solution to be brown. All the color change was thermally reversible, and the solution turned to be yellow after heating to 70 °C. The solutions also turned to be yellow after passing through a 0.2 μm PTFE, and the corresponding spectra of the filtrate showed only the peak at 454 nm, which further suggested that the absorbance at 454 nm can be assigned to the dissolved chains in coil conformation,<sup>22</sup> and the absorbance at 500–620 nm was ascribed to the nanofibers formation.<sup>23</sup> Therefore, it can be seen from Figure 1 that after nanofiber formation the number of dissolved chains in coil conformation was highest in chloroform solution and lowest in A/CF solution, and those dissolved in T/CF solution were in-between. It has been found that the solubility difference of the polymer in various solvents was correlated with the variation of microstructure in the P3HT nanofibers.<sup>17</sup> As it is known that the chloroform is a very “good” solvent for P3HT, anisole is a relatively “poor” solvent, and THF is in-between. In our experiment, the sequence of solvents that dissolve P3HT from “good” to “poor” is chloroform > T/CF > A/CF. This implied that many short chains participated in the formation of 41 nanofibers in A/CF solution, while only those chains with almost same length in chloroform attributed to the formation of monofiber.<sup>17</sup> Another interesting thing that we noted was that both 41nanofibers and 11nanofibers were formed in less than 30 min during the cooling, while it took more than 1 week for the monofiber formation. All these results suggested that there were more defects and less intrachain orders for both 41nanofibers and 11nanofibers. AFM measurements were also performed to detect the sizes of these nanofibers, which will be discussed later.

It has been found that the molecular interactions can cause either a blue- or red-shift in the absorbance spectrum and a change in the vibronic peak intensities.<sup>17</sup> In order to investigate the interactions between different P3HT nanofibers and GO, the UV-vis measurement were performed as shown in Figure 2. The detailed peak positions and  $A_{0-0}/A_{0-1}$  peak ratio in different P3HT nanostructures films and the corresponding P3HT/GO composites are summarized in Table 1. It can be seen that all the UV-vis absorption spectra of P3HT nanofiber thin films exhibited peaks at 550–560 and 600–610 nm, and nearly all the absorption spectra of P3HT/GO composites films were red-shifted more or less compared to their intrinsic P3HT films, which suggested the interactions occurred between GO and P3HT nanofibers. The shift is largest for 11nanofiber and smallest for monofiber. During the measurements, we also found that the presence of GO in the film exhibits a better light-absorbing ability, which enhanced the UV signal of the film.

It has been reported that the degree of intrachain order can be manifested in the absorbance spectra of thin films of P3HT.<sup>24–26</sup> When the polymer chains become more conjugated and the degree of intrachain order increases, the ratio of the lowest energy peak ( $A_{0-0}$ ) and next replica peak ( $A_{0-1}$ ) ( $A_{0-0}/A_{0-1}$ ) will increase.<sup>17,27</sup> Therefore, the higher  $A_{0-0}/A_{0-1}$  peak ratio means increased intrachain order and longer conjugation lengths. It can be seen from Table 1 that  $A_{0-0}/A_{0-1}$  peak ratios increased for both 41nanofibers and 11nanofibers, while the  $A_{0-0}/A_{0-1}$  peak ratio for monofiber showed little change. And the incensement extent of  $A_{0-0}/A_{0-1}$  peak ratio for P3HT/GO composites is 41nanofiber > 11nanofiber > monofiber. It has been found that GO or reduced GO (rGO) can induce P3HT to form nanofiber or

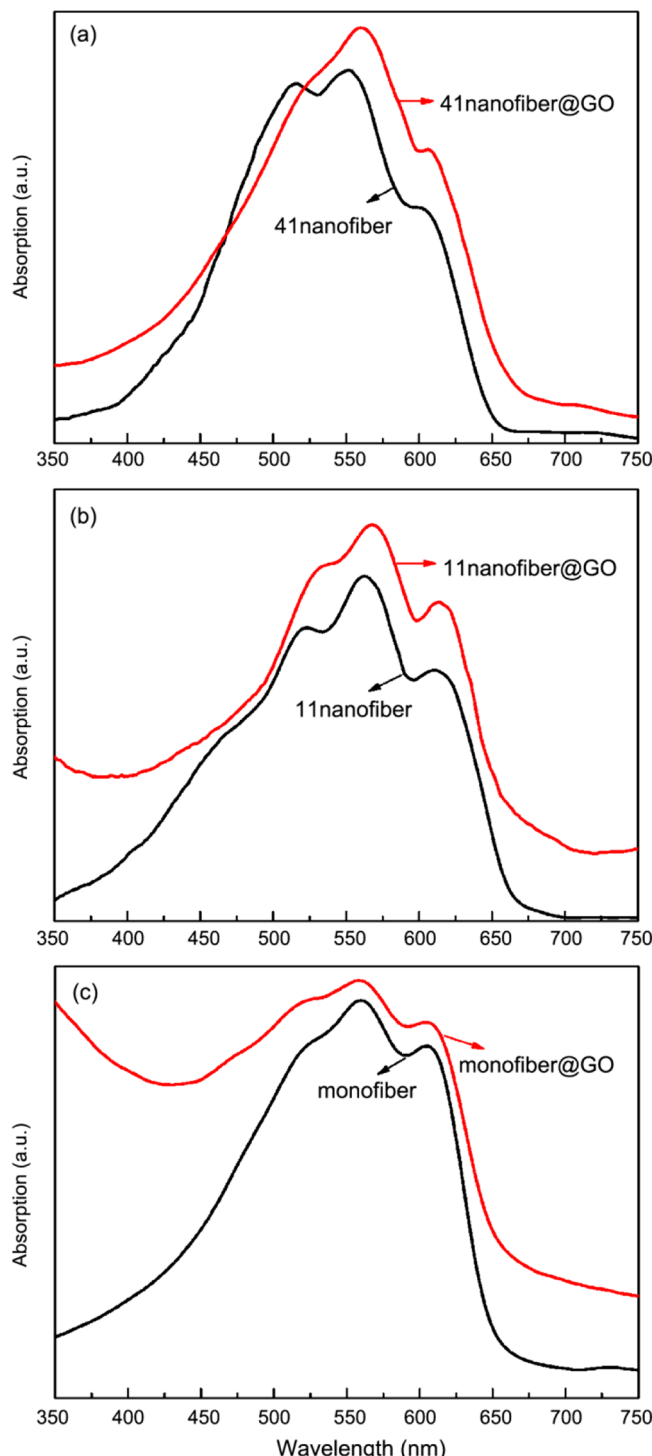


**Figure 2.** Normalized UV-vis absorption spectra of P3HT with diverse nanostructures and the corresponding P3HT/GO composite in thin solid films onto quartz substrates: (a) 41nanofiber, (b) 11nanofiber, and (c) monofiber.

nanowhisker on GO or RGO surfaces, which is time-dependent.<sup>28–30</sup> Herein, we assumed that the increase of  $A_{0-0}/A_{0-1}$  peak ratio in 41nanofiber/GO and 11nanofiber/GO composites came from the increased conjugation lengths since it is not possible that the intrachain order of P3HT nanofibers already formed is changed. In our experiment, the P3HT/GO composites films used for the UV-vis measurements were prepared by first dropping-coating GO onto the substrates and followed by dipping the substrates already coated with GO into the different P3HT solutions for some time. Then the already existed nanofibers in solution will adsorb onto the GO surface by the interactions between GO and nanofibers, and other P3HT chains existing in coil conformation in solution would move toward GO surface due to the  $\pi-\pi$  interactions between them and interact with already adsorbed nanofibers, which induced the conjugated length increased. For the monofiber/GO composites, since higher requirements, such as polymer length and longer fiber-formation time, etc., are needed, it is not possible to increase their conjugation length during the relatively short dipping process. To verify this, a time-lapse UV-vis was measured, and the obtained  $A_{0-0}/A_{0-1}$  peak ratio as a function of time is shown in Figure 3. It can be found that

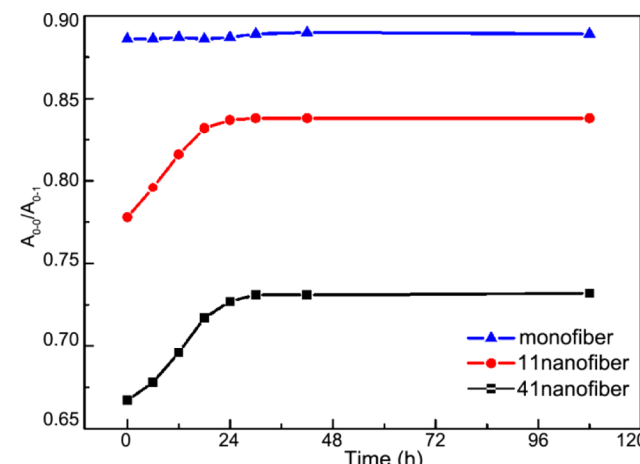


**Figure 3.**  $A_{0-0}/A_{0-1}$  UV-vis absorption spectra of thin films of P3HT with different nanostructures on quartz substrates at different hours.

for 41nanofibers and 11nanofibers the  $A_{0-0}/A_{0-1}$  peak ratio increased when the substrates coated with GO were incubated in these two P3HT solutions for more time and kept no change after 24 h, while for the monofiber the  $A_{0-0}/A_{0-1}$  showed no obvious change. This may be because the monofiber owed more high degree of crystalline, the intrachain is more ordered, and it is not easy for the shorter or longer P3HT chain to interact with the monofiber already adsorbed on the surface of GO,<sup>15</sup> while there are more chances for different-molecular-weight fraction<sup>17</sup> in A/CF and T/CF solutions to participate in the formation of nanofibers since the intrachain order of 41nanofiber and 11nanofiber is relatively less ordered.

**Table 1. Solid State UV-Vis Maxima of the  $A_{0-0}$  and  $A_{0-1}$  Transitions and  $A_{0-0}/A_{0-1}$  Ratio**

	41nanofiber	41nanofiber@GO	11nanofiber	11nanofiber@GO	monofiber	monofiber@GO
$A_{0-0}$ (nm)	602	606	610	616	606	608
$A_{0-1}$ (nm)	552	560	562	568	560	562
$A_{0-0}/A_{0-1}$	0.664	0.732	0.778	0.838	0.886	0.889

To investigate the charge-transfer interactions between different P3HT nanostructures and GO, Raman measurement were employed. Figure 4 shows the Raman spectra of different

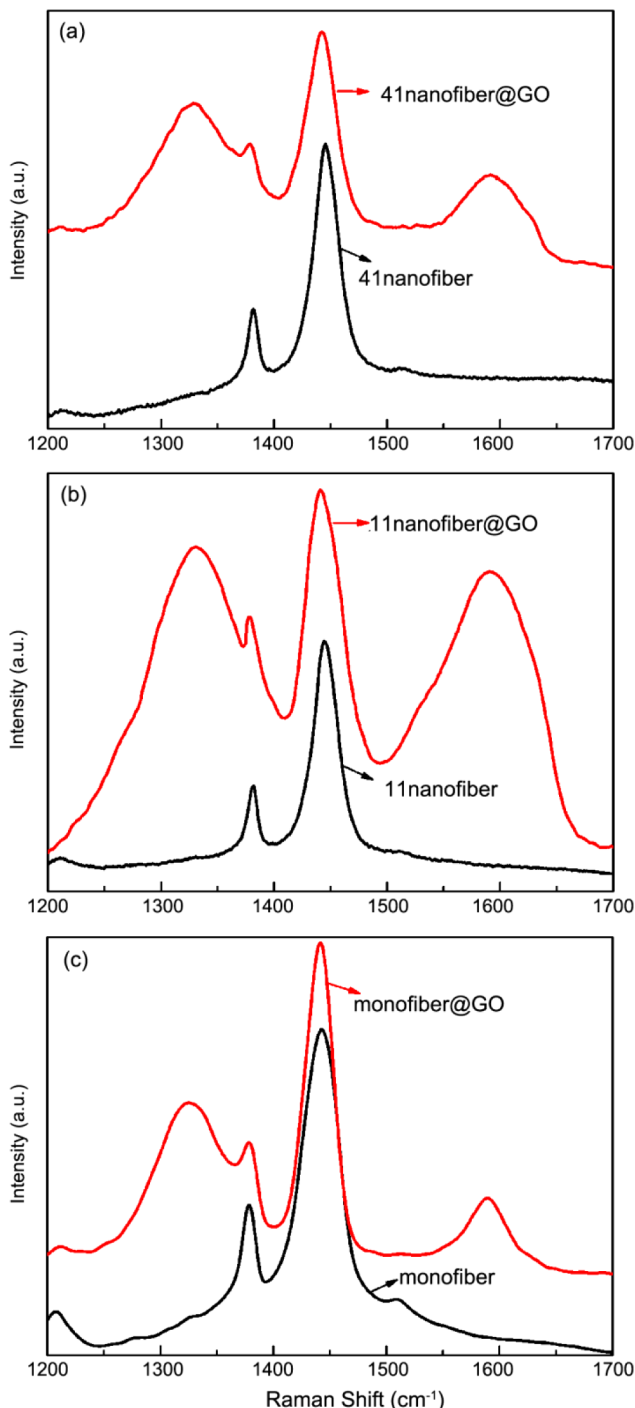


**Figure 4.** Raman spectra of different P3HT nanostructures and P3HT/GO composites: (a) 41nanofibers, (b) 11nanofibers, and (c) monofiber.

P3HT nanostructures thin films and their corresponding P3HT/GO composites films. The peak located at 1440–1450  $\text{cm}^{-1}$  is believed to come from the symmetric C=C stretching of the thiophene,<sup>31,32</sup> and the detailed C=C positions before and after the introduction of GO and G band are summarized in Table 2. It can be seen that after the introduction of GO all the C=C band in these three P3HT nanofibers shifted to lower frequencies, and the shift was largest for the 41nanofiber/GO and lowest for monofiber. It has been found that the C=C peak will shift to lower frequencies when the conjugation length in P3HT aggregates is increased.<sup>33</sup> Based on this, it is reasonable to consider that the conjugation length of P3HT nanofibers increased after adsorbing onto the surface of GO, which is consistent with the increased  $A_{0-0}/A_{0-1}$  ratio in previous UV-vis measurements and the reference results.<sup>15</sup>

The G band of pure GO film was determined to be about 1586  $\text{cm}^{-1}$ , and it was red-shifted to 1594  $\text{cm}^{-1}$  after 11nanofiber adsorbed on the GO surface, 1591  $\text{cm}^{-1}$  for 41nanofiber, and 1589  $\text{cm}^{-1}$  for monofiber. It is obvious that the position of G band varied significantly when different P3HT nanofibers were adsorbed on it. Since the position of the G band shifted proportionally to both the electron and hole concentration of graphene under electric field modulation,<sup>34,35</sup> it is reasonable to consider that different P3HT nanostructures have different influence on the electronic properties of GO, which suggested that GO was doped through interfacial charge transfer between the GO and P3HT, and the doping level of GO could be tuned by different P3HT nanostructures.

To further explore the interfacial interactions between GO and different P3HT nanostructures, structural features of the P3HT/GO composites were obtained by AFM. Figure 5 shows the large-scale AFM height images of the different P3HT nanostructures adsorbed on GO sheets. The GO sheet thickness measured by AFM was  $1.0 \pm 0.1 \text{ nm}$ , which is in good agreement with previous results.<sup>36</sup> The average sizes of P3HT monofiber were  $\sim 38 \text{ nm}$  in width and  $\sim 1.6 \text{ nm}$  in heights, which is the same as the height of a P3HT molecule in the direction of the side chains<sup>9</sup> and further confirmed that nanofibers formed in chloroform is monofibers.<sup>15</sup> The average sizes for 11nanofibers and 41nanofibers were also measured from different AFM images to be  $45 \pm 4$  and  $35 \pm 4 \text{ nm}$  in width and  $2.9 \pm 0.4$  and  $4.1 \pm 0.5 \text{ nm}$  in height, respectively. The heights of all the P3HT fibers showed no obvious change after adsorbing onto the surface of GO, which suggested that GO has no influence on the conformation of the P3HT chains in the nanofibers. From the amount of P3HT nanostructures adsorbed to the GO surfaces, it is obvious that there were attractive interactions between the GO and different P3HT nanostructures, and these attractive interactions were much stronger for 41nanofibers and 11nanofibers and relatively weaker for monofiber. When the substrates already coated with GO were dipped into different P3HT solutions, 11nanofibers preferred to adsorbing onto the surface of GO first, while the P3HT monofiber did not show this trend obviously. Relatively fewer 41nanofibers adsorbed on the GO surface compared with P3HT 11nanofibers when the substrates were incubated into

**Table 2. C=C Peaks of P3HT and P3HT/GO Composites and G Bands of GO**

	41nanofiber	41nanofiber @GO	11nanofiber	11nanofiber @GO	monofiber	monofiber @GO
C=C of P3HT	1446	1442	1444	1441	1443	1442
G band of GO		1591		1594		1589

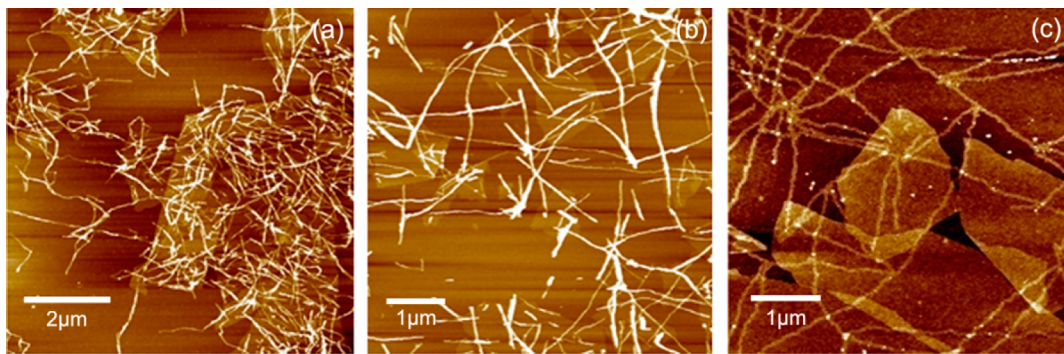


**Figure 5.** Large-scale AFM topography of different P3HT nanofibers absorbed onto the surface of GO: (a) 11nanofibers/GO, (b) 41nanofibers/GO, and (c) monofiber/GO.

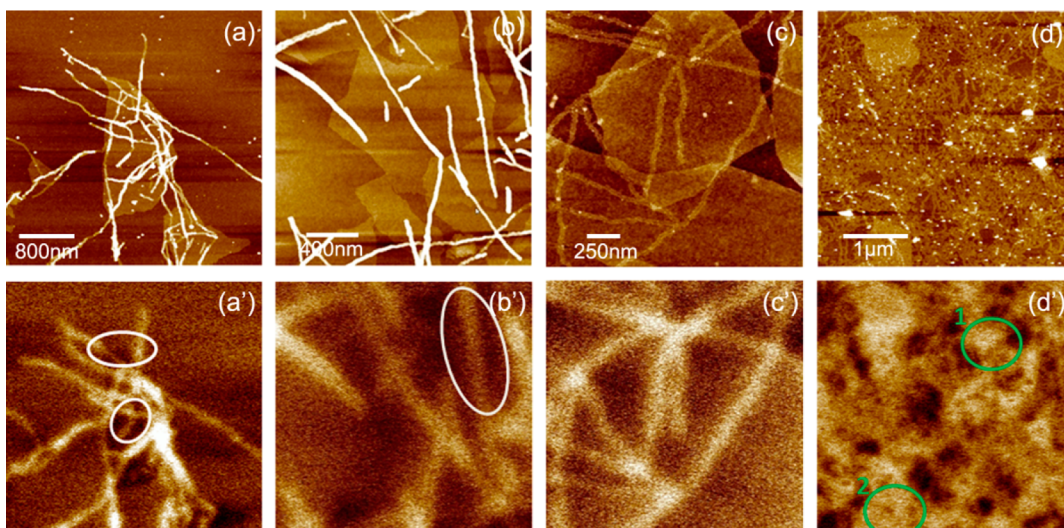


**Figure 6.** AFM (a, b, c) and KPFM (a', b', c') images of different GO–P3HT composites: (a) 11nanofibers/GO, (b) 41nanofibers/GO, and (c) monofiber/GO. The white ellipses marked some fibers with different SP contrasts. (d) AFM and (d') KPFM images of domains formed by monofiber with and without GO underneath. The green ellipses 1 and 2 mark the monofiber domain and monofiber domain @GO, respectively.

the P3HT solution for the same hours. Combined the AFM images with Raman results together, it can be easily found that the sequence of the interactions between GO and P3HT nanofibers is **11nanofiber > 41nanofiber > monofiber**.

To gain a better understanding on the interactions between GO and different P3HT nanostructures, KPFM measurements were performed. KPFM has been proved to be an important tool for studying the electrical and electronic properties of molecular thin films.<sup>37–39</sup> In KPFM, the topographic and corresponding surface potential images are obtained simultaneously, and the surface potential (SP) images provide electronic structure information.<sup>40</sup> Figure 6 displays the AFM and corresponding KPFM images of different P3HT nanostructures on the GO surface, respectively. In all these KPFM images the SiO<sub>2</sub> substrates exhibited a darker contrast, whereas the P3HT nanostructures showed a brighter contrast. However, the SP of GO showed a large variation in a range between –28 and 16 mV, which is consistent with the reference reports and can be mainly ascribed to the varying percentage of oxygen in GO and the adsorption of water on GO.<sup>18</sup> It can be found from the marked area in Figure 6 that the SP contrast of different P3HT nanostructures almost changed after adsorbed on the GO surface except for monofibers. Figure 7 records the detailed SP values of the P3HT nanostructures before and after adsorbed onto the GO. For the sake of simplicity, the substrate

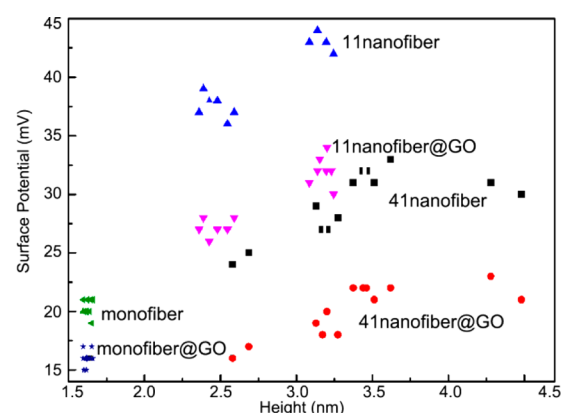


**Figure 7.** Statistical analysis of the surface potential of various P3HT nanofibers before and after they adsorbed on the GO surface.

(SiO<sub>2</sub>) was used as reference, and its SP value is level to zero. It is obvious that different nanostructures showed different surface potentials and even nanofibers with same nanostructures but different height also exhibited different surface potentials. This is reasonable since the surface potential contrast depends sensitively on the nanostructures morphology,<sup>14,25</sup> and among them 11nanofibers exhibited highest SP and monofibers have

the smallest one. The most interesting thing is that the SP contrast of P3HT nanofibers (marked by the white ellipses in Figure 6a',b') decreased after interacted with GO, and this decrease was different for different nanostructures. If the average SP contrast change was defined as  $\Delta\text{SP}$  ( $\Delta\text{SP} = \text{SP}_{\text{P3HT}} - \text{SP}_{\text{P3HT}/\text{GO}}$ ),  $\Delta\text{SP}$  was largest (about  $15 \pm 4$  mV) for 11nanofibers and smallest (about  $5 \pm 2$  mV) for monofiber. As the difference between the SP values of different P3HT nanofibers can be ascribed to different dipoles at the interface between nanofibers and the substrate,<sup>41</sup> the different  $\Delta\text{SP}$  of P3HT nanostructures suggested that the interactions between different P3HT nanostructures and GO were distinct and distinguishable by KPFM. The maximum of the potential variation of 11nanofibers implied that the interactions between 11nanofiber and GO are strongest, while the one between monofiber and GO are relatively weak. This distinguishable different interaction may be explained as following. The subtle changes in P3HT nanostructures and intrachain order can lead to the redistribution of the charges within and between the thiophene rings,<sup>14</sup> consequently changing the electronic properties of the nanofibers. Since the nanostructures of 41nanofibers/11nanofibers are different from that of monofibers, their resulted surface potentials can be different. The surface potentials of 41nanofibers differed from that of 11nanofibers, which can be due to the subtle variation in their molecular packing densities and orders. It has been known that for very thin layers the surface potential values measured is the result of complex interactions between the layers and substrates since the substrates can alter its electronic properties significantly.<sup>18,42</sup> Therefore, in our case the potential difference measured can be ascribed to the different interactions between nanofibers and GO, which were caused by different molecular packing and intrachain orders in the nanofibers. We also found that compared with the other two nanofibers, monofibers showed greater tendency to form domain or film (Figure 6d). This may be expected since the domain or film can favor the energy shift of the HOMO–LUMO with respect to the case of single fibers.<sup>37</sup> The SP of monofibers domain increased by about  $45 \pm 2$  mV compared with the single monofiber, which were almost same as the tangled 11nanofibers which usually existed in the spin-coating films. This phenomenon further supported the reported result that the average field-effect mobility of monofiber films is close to other P3HT nanofibers.<sup>15</sup> The great potential variation between the monofiber and monofiber films also implies that the intermonofiber interactions forming island are strong.

## CONCLUSIONS

In this work, we prepared several P3HT nanofibers with different nanostructures by controlling the solvent quality and concentration, which changed the intrachain order and crystalline behavior of the fibers by altering the microenvironment in which the P3HT chains aggregated. When these different P3HT nanostructures were adsorbed onto the surface of GO, the interactions between them influenced the morphology and electrical properties of the composites differently. We found that at the liquid–GO interface it was easier for the GO to interact with the nanofibers with less intrachain order and crystalline since different-molecule-weight polymer chain fractions can participate in the formation of fiber, whereas this did not apply to the monofiber with higher crystalline order and intrachain orders. At the same time the extent of surface doping of GO can be tuned by using different

P3HT nanostructures due to the different interactions between them, which was further confirmed by Raman spectroscopy. KPFM results further demonstrated that the  $\Delta\text{SP}$  was biggest among three different P3HT nanostructures, and the interactions between monofibers and monofibers are stronger than that between monofibers and GO. These findings can help understanding the interactions between GO and different P3HT nanostructures and provide more information on how to improve the charge transport across GO and conjugated polymer in polymer-based devices.

## EXPERIMENTAL SECTION

**Materials.** Regioregular P3HT ( $M_n = 34.3 \text{ kg mol}^{-1}$ , PDI = 1.24) was purchased from Rieke Metals Inc. and used without further purification. H–T regioregularity was determined using nuclear magnetic resonance to be about 98% by comparing the signals at 2.8 and 2.6 ppm.<sup>43</sup> GO were purchased from Nanjing XFNANO Materials Tech Co., Ltd. Chloroform, anisole, and THF were purchased from Beijing Chemical Reagents Company and used as received.

**Preparation of Different P3HT Nanostructures and P3HT/GO Composites.** For 41nanofibers, P3HT (1.2 mg) was added to the mixture of chloroform and anisole (volume ratio = 1:4) (10 mL), and the solution was stirred with heating (70 °C). After the P3HT was totally dissolved and the solution turned to be transparent and orange, the P3HT solution was cooled to the room temperature (the cooling rate was faster than 25 °C/h). Nanofibers mainly grow in the solution during cooling of the solution. 11nanofibers were prepared by adding a relatively poor solvent (THF) into the P3HT chloroform solution (1.2 mg mL<sup>-1</sup>). The monolayer nanowhiskers of P3HT were prepared by dissolving P3HT in chloroform at low concentration (0.14 mg mL<sup>-1</sup>) with stirring at 70 °C for some time, and then the solution were stored in darkness at room temperature for 10 days.<sup>15</sup>

Silicon wafers and quartz plates were cleaned in a boiling piranha solution ( $\text{H}_2\text{SO}_4/\text{H}_2\text{O}_2 = 7:3$  v/v) and rinsed with adequate ultrapure water. The substrates were dipped into different P3HT solutions for different times and then immediately immersed in corresponding solvents for 30 s and dried for AFM and Raman spectroscopy measurements, respectively. For preparation of P3HT/GO composites for AFM, KPFM, and Raman measurements, a drop of GO solution was first dropped onto the Si substrates and dried by temperature-controlled heating the substrates. After the Si were coated by a film of GO, they were first dipped into different P3HT solutions for different times, followed by being immersed in corresponding solvents for 30 s. All the nanostructures were used within several days after preparation.

**Characterization.** UV-vis absorption spectra were recorded on a Shimadzu UV-3600 spectrophotometer at room temperature. A P3HT solution was filled in a 2 mm thick quartz cell. Raman spectra were recorded using a LabRam HR 800 (HORIBA JobinYvon) coupled with an Olympus BX 41 microscope, and the confocal hole and the silt width were both fixed at 200  $\mu\text{m}$ . The excitation wavelength was 633 nm (He–Ne laser, 1.8 mW), and the laser was focused on the sample with a 50× objective lens. Raman signals were dispersed with a 600 lines/mm grating and collected by a charge-coupled device (CCD) camera. The spectrometer was calibrated with the 520.7 cm<sup>-1</sup> band of a Si standard.

AFM and KPFM were recorded using MultiMode AFM NanoscopeIIIa (Bruker) operated in tapping mode and lift mode, respectively. Typical AFM imaging was performed using a silicon cantilever with the resonant frequency of 300–400 kHz and radius of <10 nm. KPFM images were recorded using a conductive SCM-PIT probe (Bruker, Pt/Ir coated Si with frequency to be 75 kHz and nominal tip radius  $\leq 20$  nm).

## AUTHOR INFORMATION

### Corresponding Authors

\*E-mail: [xjma@ciac.ac.cn](mailto:xjma@ciac.ac.cn) (X.M.).

\*E-mail: [xfyu@ciac.ac.cn](mailto:xfyu@ciac.ac.cn) (X.Y.).

## Notes

The authors declare no competing financial interest.

## ACKNOWLEDGMENTS

Financial support from the Nation Natural Science Foundation of China (21304096, 21474103) is acknowledged.

## REFERENCES

- (1) Schlierf, A.; Samori, P.; Palermo, V. Graphene-organic composites for electronics: optical and electronic interactions in vacuum, liquids and thin solid films. *J. Mater. Chem. C* **2014**, *2* (17), 3129–3143.
- (2) Wang, R.; Wang, S.; Zhang, D.; Li, Z.; Fang, Y.; Qiu, X. Control of carrier type and density in exfoliated graphene by interface engineering. *ACS Nano* **2011**, *5* (1), 408–412.
- (3) Eda, G.; Chhowalla, M. Graphene-based composite thin films for electronics. *Nano Lett.* **2009**, *9* (2), 814–818.
- (4) Yin, Z.; Zhu, J.; He, Q.; Cao, X.; Tan, C.; Chen, H.; Yan, Q.; Zhang, H. Graphene-based materials for solar cell applications. *Adv. Energy Mater.* **2014**, *4* (1), 1300547.
- (5) Wang, S.; Goh, B. M.; Manga, K. K.; Bao, Q.; Yang, P.; Loh, K. P. Graphene as atomic template and structural scaffold in the synthesis of graphene-organic hybrid wire with photovoltaic properties. *ACS Nano* **2010**, *4* (10), 6180–6186.
- (6) Stylianakis, M. M.; Stratakis, E.; Koudoumas, E.; Kymakis, E.; Anastasiadis, S. H. Organic bulk heterojunction photovoltaic devices based on polythiophene-graphene composites. *ACS Appl. Mater. Interfaces* **2012**, *4* (9), 4864–4870.
- (7) El Gemayel, M.; Narita, A.; Doessel, L. F.; Sundaram, R. S.; Kiersnowski, A.; Pisula, W.; Hansen, M. R.; Ferrari, A. C.; Orgiu, E.; Feng, X.; Muellen, K.; Samor, P. Graphene nanoribbon blends with P3HT for organic electronics. *Nanoscale* **2014**, *6* (12), 6301–6314.
- (8) Yu, D.; Yang, Y.; Durstock, M.; Baek, J. B.; Dai, L. Soluble P3HT-grafted graphene for efficient bilayer-heterojunction photovoltaic devices. *ACS Nano* **2010**, *4* (10), 5633–5640.
- (9) Brinkmann, M. Structure and morphology control in thin films of regioregular poly(3-hexylthiophene). *J. Polym. Sci., Part B: Polym. Phys.* **2011**, *49* (17), 1218–1233.
- (10) Samitsu, S.; Shimomura, T.; Heike, S.; Hashizume, T.; Ito, K. Field-Effect carrier transport in poly(3-alkylthiophene) nanofiber networks and isolated nanofibers. *Macromolecules* **2010**, *43* (19), 7891–7894.
- (11) Chang, J. F.; Sun, B. Q.; Breiby, D. W.; Nielsen, M. M.; Solling, T. I.; Giles, M.; McCulloch, I.; Sirringhaus, H. Enhanced mobility of poly(3-hexylthiophene) transistors by spin-coating from high-boiling-point solvents. *Chem. Mater.* **2004**, *16* (23), 4772–4776.
- (12) Kline, R. J.; McGehee, M. D.; Toney, M. F. Highly oriented crystals at the buried interface in polythiophene thin-film transistors. *Nat. Mater.* **2006**, *5* (3), 222–228.
- (13) Zhang, R.; Li, B.; Iovu, M. C.; Jeffries-El, M.; Sauve, G.; Cooper, J.; Jia, S. J.; Tristram-Nagle, S.; Smilgies, D. M.; Lambeth, D. N.; McCullough, R. D.; Kowalewski, T. Nanostructure dependence of field-effect mobility in regioregular poly(3-hexylthiophene) thin film field effect transistors. *J. Am. Chem. Soc.* **2006**, *128* (11), 3480–3481.
- (14) Baghgar, M.; Barnes, A. M.; Pentzer, E.; Wise, A. J.; Hammer, B. A. G.; Emrick, T.; Dinsmore, A. D.; Barnes, M. D. Morphology-dependent electronic properties in cross-linked (P3HT-b-P3MT) block copolymer nanostructures. *ACS Nano* **2014**, *8* (8), 8344–8349.
- (15) Guo, Y.; Jiang, L.; Ma, X.; Hu, W.; Su, Z. Poly(3-hexylthiophene) monolayer nanowiskers. *Polym. Chem.* **2013**, *4* (16), 4308–4311.
- (16) Liu, J.; Arif, M.; Zou, J.; Khondaker, S. I.; Zhai, L. Controlling poly(3-hexylthiophene) crystal dimension: nanowiskers and nano-ribbons. *Macromolecules* **2009**, *42* (24), 9390–9393.
- (17) Roehling, J. D.; Arslan, I.; Moule, A. J. Controlling microstructure in poly(3-hexylthiophene) nanofibers. *J. Mater. Chem.* **2012**, *22* (6), 2498–2506.
- (18) Liscio, A.; Veronese, G. P.; Treossi, E.; Suriano, F.; Rossella, F.; Bellani, V.; Rizzoli, R.; Samori, P.; Palermo, V. Charge transport in graphene-polythiophene blends as studied by Kelvin Probe Force Microscopy and transistor characterization. *J. Mater. Chem.* **2011**, *21* (9), 2924–2931.
- (19) Liu, Q.; Liu, Z.; Zhong, X.; Yang, L.; Zhang, N.; Pan, G.; Yin, S.; Chen, Y.; Wei, J. Polymer photovoltaic cells based on solution-processable graphene and P3HT. *Adv. Funct. Mater.* **2009**, *19* (6), 894–904.
- (20) Gao, Y.; Yip, H. L.; Chen, K. S.; O’Malley, K. M.; Acton, O.; Sun, Y.; Ting, G.; Chen, H.; Jen, A. K. Y. Surface doping of conjugated polymers by graphene oxide and its application for organic electronic devices. *Adv. Mater.* **2011**, *23* (16), 1903–1908.
- (21) Wang, S.; Nai, C. T.; Jiang, X. F.; Pan, Y.; Tan, C. H.; Nesladek, M.; Xu, Q. H.; Loh, K. P. Graphene oxide-polythiophene hybrid with broad-band absorption and photocatalytic properties. *J. Phys. Chem. Lett.* **2012**, *3* (17), 2332–2336.
- (22) Rughooputh, S.; Hotta, S.; Heeger, A. J.; Wudl, F. Chromism of soluble polythienylenes. *J. Polym. Sci., Part B: Polym. Phys.* **1987**, *25* (5), 1071–1078.
- (23) Samitsu, S.; Shimomura, T.; Heike, S.; Hashizume, T.; Ito, K. Effective production of poly(3-alkylthiophene) nanofibers by means of Whisker method using anisole solvent: structural, optical, and electrical properties. *Macromolecules* **2008**, *41* (21), 8000–8010.
- (24) Spano, F. C. Modeling disorder in polymer aggregates: The optical spectroscopy of regioregular poly(3-hexylthiophene) thin films. *J. Chem. Phys.* **2005**, *122* (23), 234701.
- (25) Chang, J. F.; Clark, J.; Zhao, N.; Sirringhaus, H.; Breiby, D. W.; Andreassen, J. W.; Nielsen, M. M.; Giles, M.; Heeney, M.; McCulloch, I. Molecular-weight dependence of interchain polaron delocalization and exciton bandwidth in high-mobility conjugated polymers. *Phys. Rev. B: Condens. Matter Mater. Phys.* **2006**, *74* (11), 115318.
- (26) Spano, F. C. Absorption in regio-regular poly(3-hexylthiophene) thin films: Fermi resonances, interband coupling and disorder. *Chem. Phys.* **2006**, *325* (1), 22–35.
- (27) Spano, F. C. The spectral signatures of Frenkel polarons in H- and J-aggregates. *Acc. Chem. Res.* **2010**, *43* (3), 429–439.
- (28) Zhou, X.; Yang, X. Improved dispersibility of graphene oxide in o-dichlorobenzene by adding a poly(3-alkylthiophene). *Carbon* **2012**, *50* (12), 4566–4572.
- (29) Chunder, A.; Liu, J.; Zhai, L. Reduced graphene oxide/poly(3-hexylthiophene) supramolecular composites. *Macromol. Rapid Commun.* **2010**, *31* (4), 380–384.
- (30) Yang, Z.; Shi, X.; Yuan, J.; Pu, H.; Liu, Y. Preparation of poly(3-hexylthiophene)/graphene nanocomposite via in situ reduction of modified graphite oxide sheets. *Appl. Surf. Sci.* **2010**, *257* (1), 138–142.
- (31) Louarn, G.; Trznadel, M.; Buisson, J. P.; Laska, J.; Pron, A.; Lapkowski, M.; Lefrant, S. Raman spectroscopic studies of regioregular poly(3-alkylthiophenes). *J. Phys. Chem.* **1996**, *100* (30), 12532–12539.
- (32) Baibarac, M.; Lapkowski, M.; Pron, A.; Lefrant, S.; Baltog, I. SERS spectra of poly(3-hexylthiophene) in oxidized and unoxidized states. *J. Raman Spectrosc.* **1998**, *29* (9), 825–832.
- (33) Tsoi, W. C.; James, D. T.; Kim, J. S.; Nicholson, P. G.; Murphy, C. E.; Bradley, D. D. C.; Nelson, J.; Kim, J. S. The nature of in-plane skeleton raman modes of P3HT and their correlation to the degree of molecular order in P3HT:PCBM blend thin films. *J. Am. Chem. Soc.* **2011**, *133* (25), 9834–9843.
- (34) Das, A.; Pisana, S.; Chakraborty, B.; Piscanec, S.; Saha, S. K.; Waghmare, U. V.; Novoselov, K. S.; Krishnamurthy, H. R.; Geim, A. K.; Ferrari, A. C.; Sood, A. K. Monitoring dopants by Raman scattering in an electrochemically top-gated graphene transistor. *Nat. Nanotechnol.* **2008**, *3* (4), 210–215.
- (35) Yan, J.; Zhang, Y.; Kim, P.; Pinczuk, A. Electric field effect tuning of electron-phonon coupling in graphene. *Phys. Rev. Lett.* **2007**, *98* (16), 166802.
- (36) Treossi, E.; Melucci, M.; Liscio, A.; Gazzano, M.; Samori, P.; Palermo, V. High-contrast visualization of graphene oxide on dye-

- sensitized glass, quartz, and silicon by fluorescence quenching. *J. Am. Chem. Soc.* **2009**, *131* (43), 15576–15577.
- (37) Liscio, A.; Palermo, V.; Samori, P. Probing local surface potential of quasi-one-dimensional systems: a KPFM study of P3HT nanofibers. *Adv. Funct. Mater.* **2008**, *18* (6), 907–914.
- (38) Liscio, A.; Palermo, V.; Gentilini, D.; Nolde, F.; Müllen, K.; Samori, P. Quantitative measurement of the local surface potential of pi-conjugated nanostructures: a Kelvin Probe Force Microscopy study. *Adv. Funct. Mater.* **2006**, *16* (11), 1407–1416.
- (39) Palermo, V.; Palma, M.; Samori, P. Electronic characterization of organic thin films by Kelvin Probe Force Microscopy. *Adv. Mater.* **2006**, *18* (2), 145–164.
- (40) Liscio, A.; Palermo, V.; Samori, P. Nanoscale quantitative measurement of the potential of charged nanostructures by electrostatic and Kelvin Probe Force Microscopy: unraveling electronic processes in complex materials. *Acc. Chem. Res.* **2010**, *43* (4), 541–550.
- (41) Saito, N.; Hayashi, K.; Sugimura, H.; Takai, O.; Nakagiri, N. Surface potential images of self-assembled monolayers patterned by organosilanes: ab initio molecular orbital calculations. *Surf. Interface Anal.* **2002**, *34* (1), 601–605.
- (42) Giovannetti, G.; Khomyakov, P. A.; Brocks, G.; Karpan, V. M.; van den Brink, J.; Kelly, P. J. Doping graphene with metal contacts. *Phys. Rev. Lett.* **2008**, *101*, 026803.
- (43) Sirringhaus, H.; Brown, P. J.; Friend, R. H.; Nielsen, M. M.; Bechgaard, K.; Langeveld-Voss, B. M. W.; Spiering, A. J. H.; Janssen, R. A. J.; Meijer, E. W.; Herwig, P.; de Leeuw, D. M. Two-dimensional charge transport in self-organized, high-mobility conjugated polymers. *Nature* **1999**, *401* (6754), 685–688.